# Probability of the Emergence of Helical Precipitation Patterns in the Wake of Reaction-Diffusion Fronts

Shibi Thomas,[1,*] István Lagzi,[2,†] Ferenc Molnár, Jr.,[3,‡] and Zoltán Rácz[4,§]

[1]*Department of Theoretical Physics, Eötvös University, 1117 Budapest, Hungary*
[2]*Department of Physics, Budapest University of Technology and Economics, 1111 Budapest, Hungary*
[3]*Department of Physics, Applied Physics, and Astronomy, Rensselaer Polytechnic Institute, Troy, 12180 New York, USA*
[4]*Institute for Theoretical Physics—HAS, Eötvös University, 1117 Budapest, Hungary*

(Received 11 September 2012; published 13 February 2013)

Helical and helicoidal precipitation patterns emerging in the wake of reaction-diffusion fronts are studied. In our experiments, these chiral structures arise with well-defined probabilities $P_H$ controlled by conditions such as, e.g., the initial concentration of the reagents. We develop a model which describes the observed experimental trends. The results suggest that $P_H$ is determined by a delicate interplay among the time and length scales related to the front and to the unstable precipitation modes and, furthermore, that the noise amplitude also plays a quantifiable role.

DOI: 10.1103/PhysRevLett.110.078303 PACS numbers: 82.40.Ck, 02.50.−r, 05.40.−a, 68.35.Ct

Helices and helicoids are present from the nanoscale to the macroscale (ZnO nanohelices [1], macromolecules and inorganic crystals with a helical structure [2,3], precipitation helices [4–6], fiber geometry of heart walls [7]). The formation of these fascinating structures generally follows two routes. First, templates with chiral symmetry (e.g., oragogel fibers) may exist in the system, and the symmetry is just transcribed to a structure (e.g., inorganic materials [8]) at a larger scale. Second, spontaneous symmetry breaking may occur through the self-assembly of achiral building blocks into a helical or helicoidal structure, such as, e.g., in the case of crystals with chiral morphology [2,9].

Theoretically, the symmetry-breaking route is more interesting. Universal aspects may emerge, and the robust features of this self-organization process may be important for applications as well. Indeed, control over creating helical structures would make engineering (in particular, the bottom-up design of micropatterns [10]) more flexible since chiral morphology of materials is known to affect their physical (electronic) properties [6,11].

In order to develop insight into the genesis of helices or helicoids, we investigate an emblematic example of pattern formation, namely, the formation of precipitation patterns in the wake of reaction-diffusion fronts [12,13]. The motivation for this choice comes from the observation that helicoidal structures have an axis, and the correlations are simple in the plane perpendicular to the axis. This suggests that building the perpendicular correlations in the wake of an advancing planar front may be a simple and natural mechanism of creating helices or helicoids. Additional motivation comes from the existence of a large body of knowledge in the related Liesegang phenomena [12,13]. It allows the use of well-established experimental and theoretical approaches, thus making it easier to develop a novel view on the formation of helical structures.

Our main results concern the probabilistic aspects of the symmetry-breaking route. We determine the probability $P_H$ of the emergence of single helices or helicoids in Liesegang-type experiments as the conditions such as the initial concentration of inner or outer electrolytes or the temperature are changed. $P_H$ is found to be well reproducible and large ($P_H > 0.5$ for some parameter range). The results are understood by expanding and simulating a model of formation of precipitation patterns [14]. We explicitly observe that the origin of helices or helicoids is not to be found in the fluctuations and asymmetry of the initial or boundary conditions [15,16]. Instead, the growth of unstable modes, the dynamics of the front, and the bulk fluctuations (noise) combine to yield the helices.

In our experiments, we study the precipitation reaction $Cu^{2+}(aq) + CrO_4^{2-}(aq) \rightarrow CuCrO_4(s)$ in 1% agarose gel. The gel soaked with $K_2CrO_4$ (inner electrolyte) is placed in a test tube, and a solution of $CuCl_2$ (outer electrolyte) is poured on top of the gel. Setting the concentration of the outer electrolyte an order of magnitude larger than that of the inner electrolyte yields a reaction front diffusing into the gel, and a Liesegang pattern of precipitation bands forms behind the front (Fig. 1). Frequently, however, helicoids evolve from the same macroscopic experimental conditions (Fig. 1). We quantified the stochastic nature of this intriguing phenomenon by varying the concentration of the outer ($a_0$) and inner ($b_0$) electrolytes, the radius of the test tube ($R$), and the temperature ($T$) and by measuring $P_H$ using 10 independent experiments for each parameter set.

Similar experiments were carried out in a quasi-two-dimensional geometry as well. The gel (with the inner electrolyte $B$) was placed in the gap between two test tubes of slightly different radii ($\delta R = 2$ mm), thus effectively confining the pattern to the surface of a cylinder (Fig. 2). In this geometry, we observed the formation of regular

 

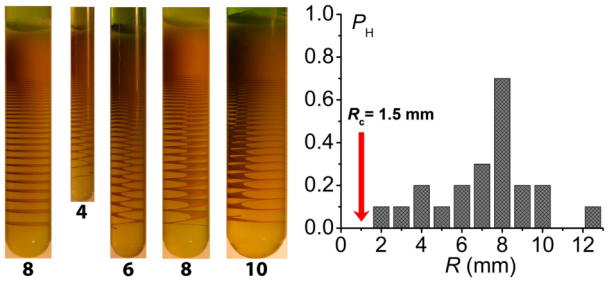


FIG. 1 (color online). Regular Liesegang (leftmost tube) and helicoidal (all other tubes) patterns in agarose gel with the numbers corresponding to the tube radius $R$ measured in mm. $R$ is varied at fixed experimental conditions ($T = 22\,^{\circ}$C, $[Cu^{2+}]_0 = a_0 = 0.5$ M, and $[CrO_4^{2-}]_0 = b_0 = 0.01$ M), and the probability of helicoid formation $P_H$ is displayed (right panel). No helicoid appears for $R \leq R_c$.

Liesegang rings, single helices, double helices, and more complex patterns for large $R$.

Figure 1 shows regular bands and helicoidal patterns in test tubes of various radii, together with the measured probability of helicoid formation ($P_H$). We observe no helicoids below a critical radius ($R_c = 1.5$ mm), in agreement with theoretical expectations based on a simplified model where the reaction front moves with fixed velocity [15,16]. For $R > R_c$, one finds that $P_H$ increases with increasing $R$ and reaches rather large values ($P_H \approx 0.7$ at $R = 8$ mm) before decreasing again. The decrease at large $R$ is due to the noticeable proliferation of complex structures (double or triple helicoids, disordered patterns) which suppress the weight of single helicoids.

Before describing the experiments further, we turn to the theory since it allows a more concise discussion of the results. Theories of Liesegang-type patterns combine the properties of a moving front (i.e., where and at what rate the reaction product, $A + B \rightarrow C$, appears) with the details

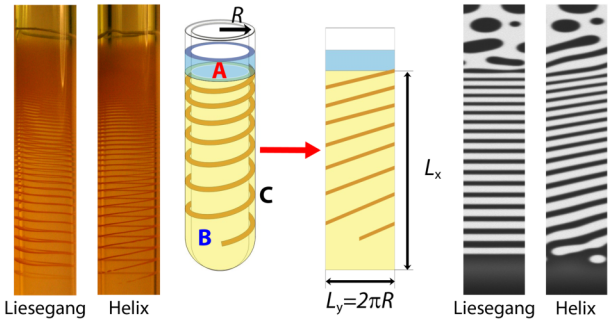


FIG. 2 (color online). Transformation of the thin layer of gel in the *tube-in-tube* experiment into a two-dimensional strip. The Liesegang bands and the helices in the experiments were obtained in agarose gel at $T = 22\,^{\circ}$C, $a_0 = 0.5$ M, and $b_0 = 0.01$ M, with the radii of the outer and inner tubes being 8 and 6 mm. The scaled parameters used for the simulations (columns on the right, with the precipitate shown in white) were $a_0 = 80$, $b_0 = 1$, $\sigma = 0.8$, $\lambda = 0.2$, $\eta = 0.05$, and $L_y = 64$.

of the precipitation (i.e., how the reaction product, $C$, turns into precipitate). While the front properties have been thoroughly studied and understood both theoretically [17,18] and experimentally [19,20], the dynamics of precipitation is more debated [13,18]. The competing pre- and postnucleation views can be combined [18,21], and we shall use a simple version [14] based on the Cahn-Hilliard equation with noise added [22–24]. This equation features spinodal-decomposition-type fast dynamics, as well as slower nucleation-and-growth processes [25]. Driving it with a reaction zone gives us a flexible model with a variety of pattern-formation regimes.

The reaction front appears due to a strongly inhomogeneous initial distribution of the reagents $A$ and $B$. The reaction takes place in a gel (occupying the half space $x > 0$), and, initially, the inner electrolyte $B$ is homogeneously distributed [$b(x > 0, y, t = 0) = b_0$]. The outer electrolyte $A$ of much higher concentration [$a(x < 0, y, t = 0) = a_0$ with $a_0 \gg b_0$] is brought into contact with the gel at $t = 0$. Assuming a second-order irreversible reaction $A + B \rightarrow C$, the front invading the gel can be described by the equations

$$\partial_t a = D_A \Delta a - kab, \tag{1}$$

$$\partial_t b = D_B \Delta b - kab, \tag{2}$$

where both the reaction rate $k$ and the diffusion coefficients, which are assumed to be equal ($D_A = D_B = D$), are set to 1 by an appropriate choice of the time and length scales [26]. The front, specified in terms of the rate of production of $C$'s ($kab$), is narrow and moves into the gel diffusively. Its position is given by $x_f = \sqrt{2D_f t}$, where $D_f$ is a function of $D$ and $b_0/a_0$. The front leaves behind a constant concentration of $C$'s ($c_0$), where $c_0$ depends on $D$ and $b_0/a_0$, and it is practically independent of $k$. Provided the system with $c_0$ is unstable or metastable, a phase separation of $C$'s into regions of high ($c_h$) and low ($c_\ell$) concentrations takes place. This process is described by the Cahn-Hilliard equation with source ($kab$) and noise ($\eta_c$) terms added:

$$\partial_t m = -\lambda \Delta (m - m^3 + \sigma \Delta m) + kab + \eta_c. \tag{3}$$

Here, $m$ is the concentration of $C$'s shifted by $\bar{c} = (c_h + c_\ell)/2$ and scaled by $\hat{c} = (c_h - c_\ell)/2$, so that $m = (c - \bar{c})/\hat{c}$ is 1 for $c = c_h$ and $m = -1$ for $c = c_\ell$. The parameters $\lambda$ and $\sigma$ are the rescaled kinetic coefficient and surface tension, respectively [14,23,24]. Their ratio $\tau_u \approx \sigma/\lambda$ defines a characteristic time scale of the growth of unstable modes in precipitation. Comparing $\tau_u$ with the time the front passes through a region determines whether slow nucleation-and-growth or fast spinodal decomposition dominates the pattern formation.

Adding noise ($\eta_c$) is essential since the formation of helices is a symmetry-breaking process. Furthermore, the noise widens the available regions of the meta- and

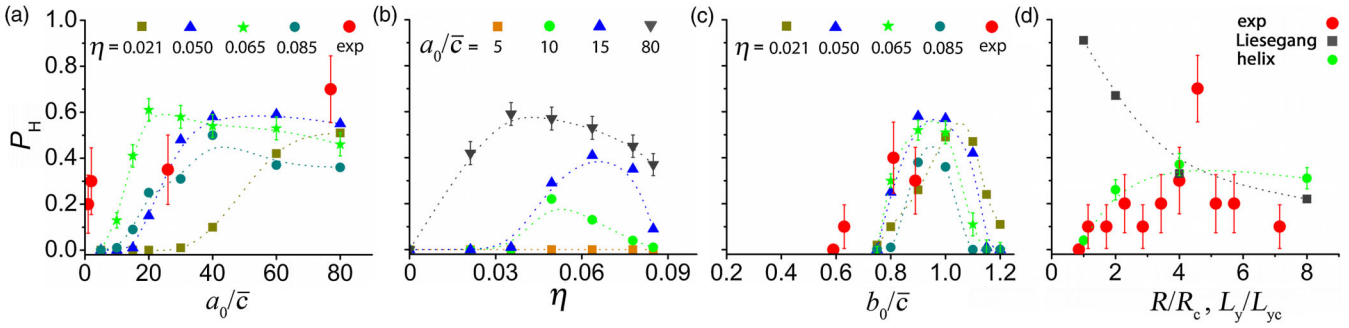


FIG. 3 (color online). The probability of helicoid or helix formation $P_H$ in experiments (large red dots) and in simulations (small symbols). Displayed are the dependence [(a) and (c)] on the outer and inner electrolyte concentrations, (b) on the noise amplitude, and (d) on the radius (width) of the system. The values of the parameters kept fixed in a panel, and the experimental estimate of the scale factor $\bar{c}$ are discussed in the text. Statistical errors are shown for the experiments and for a single set of simulations.

unstable states (see earlier morphological phase diagrams of Liesegang patterns [27]). Noiseless Cahn-Hilliard-type dynamics where the front moves with *fixed velocity* have been much studied [28,29]. In these cases, however, noise was present in the initial state and complex morphologies resulted from complex initial conditions or from complex motion of the reaction front. Our model without the noise reproduces the properties of the regular Liesegang patterns [14,30]. Inclusion of the bulk noise allows us to demonstrate the existence of helices and to understand the experimental trends in their emergence.

From a theoretical point of view, the *tube-in-tube* experiments are the easiest to describe. We can cut and open the cylinder as shown in Fig. 2 and treat the thin layer as a two-dimensional strip of width $L_y = 2\pi R$ and length equal to the tube length $L_x$ [31]. Accordingly, Eqs. (1)–(3) are solved in a rectangle of size $L_x \times L_y$ with periodic boundary conditions in the $y$ direction and no-flux boundary conditions at the lower edge ($x = L_x$, $y$). At the upper edge [the initial location of the front ($x = 0$, $y$)], we use a slightly idealized boundary: The concentration of the outer electrolyte is kept at a constant value $a(x = 0, y, t) = a_0/\bar{c}$ while the no-flux condition is adopted for $B$ and $C$. The initial conditions reflect the experimental setup: $b(x > 0, y, t = 0) = b_0/\bar{c}$, $a(x > 0, y, t = 0) = 0$, and $c(x, y, t = 0) = 0$. The discretized noise term $\eta_c$ is implemented by moving $C$'s between neighboring sites at a rate $\eta_c = \sqrt{c}r$, where $r$ is uniformly distributed in the interval $[-\eta, \eta]$. In the following, $\eta$ is called the amplitude of the noise.

Our simulations indicate that both the Liesegang bands and the helices emerge in a wide range of the parameters. There are, of course, some constraints, e.g., $\eta$ must be sufficiently small for the phase separation to take place. Examples of simulations are shown in Fig. 2 (rightmost two columns), where a Liesegang pattern and a helix are displayed [26]. A general feature of the simulations is that the chirality of the helices is random within the statistical error of 100 independent simulations. This is in agreement with the experiments where, out of 96 helicoids or helices, the ratio of left- and right-handed patterns is 50/46. We consider this as experimental evidence that the macroscopic symmetry breaking is not driven by microscopic objects of a given chirality.

To characterize the emergence of the helices quantitatively, we collected data by varying $a_0$, $b_0$, $\eta$, and $L_y$ and determined $P_H$ from the outcome of 100 simulations with distinct random number sequences for $\eta_c$. Since the kinetic coefficients $\lambda$ and $\sigma$ cannot be controlled externally, we kept them fixed ($\lambda = 0.2$, $\sigma = 0.8$) throughout the simulations.

First, we varied $a_0/\bar{c}$ and $\eta$ while keeping $b_0/\bar{c} = 1$ and $L_y = 64$ fixed. Figures 3(a) and 3(b) show that $P_H$ is remarkably large; it increases with $a_0$ and reaches $P_H \sim 0.4$–$0.6$ for large $a_0/\bar{c}$. A similar trend is also seen in the experiments. Since $a_0/b_0$ determines the front motion, with larger $a_0$ corresponding to faster diffusion, an important conclusion from Fig. 3(a) is that the fast motion of the front facilitates the emergence of helices.

Figures 3(a) and 3(b) also show that no helices form even for larger $a_0/\bar{c}$ if the noise is too small. Increasing the noise first increases $P_H$; then, $P_H$ saturates in the region $0.05 < \eta < 0.09$; finally, $P_H \to 0$ due to the absence of phase separation above $\eta \approx 0.09$. Comparing Fig. 3(b) with experiments is difficult since the link between $\eta$ and $T$ is through complex changes in diffusion, reaction rates, etc. Our experiments indicate that $P_H$ increases with $T$. This is in agreement with Fig. 3(b), provided $\eta \sim T$ and the experimental $T$ corresponds to small values of $\eta$.

We also varied $b_0/\bar{c}$ and $\eta$ while fixing $a_0/\bar{c} = 80$ and $L_y = 64$ [Fig. 3(c)]. The probability $P_H$ was found to be maximal in the middle of the spinodal region ($b_0/\bar{c} \approx 0.9$–$1.1$), where isotropic precipitation structures develop through fast-growing linearly unstable modes. Comparing the simulations [Fig. 3(c)] with experiments is difficult since neither $\eta$ nor the experimental concentration scale, $\bar{c} = (c_h + c_\ell)/2 \approx c_h/2$, are known. We estimated $c_h$ by assuming that all the precipitate was in the helices, and all

the $B$'s reacted and turned into $C$'s. This estimate left an apparent shift between the experimental and simulation points [Fig. 3(c)]. The shift may well be the consequence of overestimating $c_h$ (e.g., not all the $B$'s reacted or the bands are wider than their optical width).

The effect of increasing width ($L_y$) is displayed in Fig. 3(d). The experimental parameters are described in Fig. 1, while, in simulations, we used $a_0/\bar{c} = 15$, $b_0/\bar{c} = 1$, and $\eta = 0.04$. The experimentally observed lower threshold for the emergence of helices is clearly present ($L_{yc} \approx 32$), and one can also recognize the trend that $P_H$ first increases with $L_y$ and then decreases for large $L_y$. As in experiments, $P_H$ decreases due to the proliferation of more complex structures. Complexity builds up for large $L_y$ since more long-wavelength transverse modes (modes in the $y$ direction) can fit into the system. They are unstable modes of the Cahn-Hilliard dynamics facilitating the formation of more intricate patterns.

The common trends found in experiments and simulations suggest that our model contains the right ingredients, and we can develop a physical picture of helix formation by observing the simulations. Figure 4 displays two examples of time evolutions with parameters set to have roughly equal probabilities for bands and helices. There are many ways of choosing such parameters, but the characteristic features of the dynamics are always the same. Essential among them is that, initially, the reaction front moves fast enough to produce a domain where the system is unstable and roughly homogeneous (fuzzy regions in the $t = 720$–$960$ plates in Fig. 4). The homogeneity makes possible the generation of isotropic patterns which compete with the anisotropic influence of the front favoring band formation perpendicular to the front motion ($t = 1440$–$1920$ plates in Fig. 4). The outcome of this competition determines whether Liesegang bands, single helix, double helix, or more complicated patterns emerge.

One can quantify the above picture by noting that homogeneous patterns can form only if the front moves a distance of the order $L_y$ in a time $\tau_f = L_y^2/2D_f$ that is smaller than the time, $\tau_u$, required for the precipitation to develop. To estimate $\tau_u$, we calculate the growth rate, $\omega_{k^*} = \lambda/4\sigma \approx 1/\tau_u$, of the fastest-growing mode of wave number $k^* = 1/\sqrt{2\sigma}$ using linearized Cahn-Hilliard dynamics for a quench to the middle of the miscibility gap [$m(0) \approx 0$]. Then, assuming that the homogeneous structure emerges from the noise, we have $\sqrt{\eta}\exp(\omega_{k^*}\tau_u) \approx m(\tau_u) \approx 1$, and the inequality $\tau_f < \tau_u$ yields an upper limit for the width of a system $L_y^2 < 4D_f\sigma|\ln\eta|/\lambda$ where a helix can form. A lower limit can also be found since the characteristic size of the domains ($L^* \approx 2\pi/k^* = 2\pi\sqrt{2\sigma}$) formed by the fastest-growing modes must be smaller that the width of the system ($L^* < L_y$); otherwise, no structure forms in the $y$ direction. The combination of the two inequalities

$$8\pi^2\sigma < L_y^2 < 4D_f\sigma|\ln\eta|/\lambda \qquad (4)$$

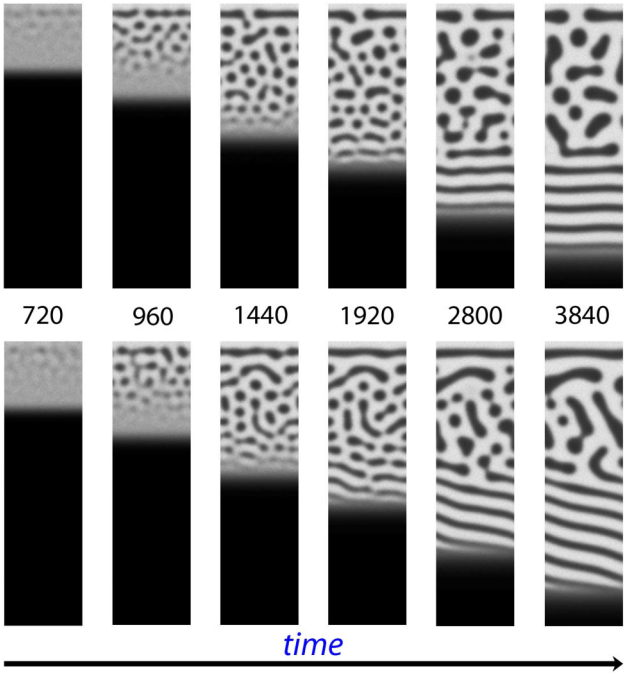


FIG. 4 (color online). Time evolution of the precipitate (white regions) for parameters $a_0/\bar{c} = 60$, $b_0/\bar{c} = 1$, $\eta = 0.02$, and $L_y = 64$.

reflects some of the trends observed in the experiments and simulations. Namely, the formation of helices is facilitated by a fast moving front, i.e., by $D_f$ being large, which, in turn, requires $a_0$ to be large; furthermore, there is a minimal width below which no helices form.

Since the width ($L_y$) is bounded from both sides, it may happen that no helices can form. When searching for helices, one should, in general, use a fast front (e.g., by selecting large $a_0$) and create an unstable state behind the front by placing the system deep in the miscibility gap (e.g., by experimenting with $b_0$). Finding the right temperatures is also important, but it is a rather complex problem left for future studies.

This work was funded by the Hungarian Academy of Sciences through OTKA Grants No. K68109, No. NK100296, and No. K104990. F. M. acknowledges partial support by the NSF through Grant No. DEB-0918413.

*Present address: Department of Physics, University of Calicut, 673635 Kerala, India.
shibithomas969@gmail.com
†istvanlagzi@gmail.com
‡molnaf@rpi.edu
§racz@general.elte.hu

[1] P. X. Gao, Y. Ding, W. J. Mai, W. L. Hughes, C. S. Lao, and Z. L. Wang, Science **309**, 1700 (2005).
[2] H. Imai, and Y. Oaki, Angew. Chem., Int. Ed. Engl. **43**, 1363 (2004).

[3] D. S. Su, Angew. Chem., Int. Ed. Engl. **50**, 4747 (2011).
[4] S. C. Müller, S. Kai, and J. Ross, Science **216**, 635 (1982).
[5] R. V. Suganthi, E. K. Girija, S. Narayana Kalkura, H. K. Varma, and A. Rajaram, J. Mater. Sci. Mater. Med. **20**, 131 (2009).
[6] O. Giraldo, S. L. Brock, M. Marquez, S. L. Suib, H. Hillhouse, and M. Tsapatsis, Nature (London) **405**, 38 (2000).
[7] P. Savadjiev, G. J. Strijkers, A. J. Bakermans, E. Piuze, S. W. Zucker, and K Siddiqi, Proc. Natl. Acad. Sci. U.S.A. **109**, 9248 (2012).
[8] J. H. Jung, Y. Ono, K. Hanabusa, and S. Shinkai, J. Am. Chem. Soc. **122**, 5008 (2000).
[9] Y. Oaki and H. Imai, J. Am. Chem. Soc. **126**, 9271 (2004).
[10] B. A. Grzybowski, K. J. M. Bishop, C. J. Campbell, M. Fialkowski, and S. K. Smoukov, Soft Matter **1**, 114 (2005).
[11] S. Y. Ju, J. Doll, I. Sharma, and F. Papadimitrakopoulos, Nat. Nanotechnol. **3**, 356 (2008).
[12] H. K. Henisch, *Crystals in Gels and Liesegang Rings* (Cambridge University Press, Cambridge, England, 1988).
[13] S. C. Müller and J. Ross, J. Phys. Chem. A **107**, 7997 (2003).
[14] T. Antal, M. Droz, J. Magnin, and Z. Rácz, Phys. Rev. Lett. **83**, 2880 (1999).
[15] D. S. Chernavskii, A. A. Polezhaev, and S. C. Müller, Physica (Amsterdam) **54D**, 160 (1991).
[16] A. A. Polezhaev and S. C. Müller, Chaos **4**, 631 (1994).
[17] L. Gálfi and Z. Rácz, Phys. Rev. A **38**, 3151 (1988).
[18] T. Antal, M. Droz, J. Magnin, Z. Rácz, and M. Zrinyi, J. Chem. Phys. **109**, 9479 (1998).
[19] C. Léger, F. Argoul, M. Bazant, and J. Argoul, J. Phys. Chem. B **103**, 5841 (1999).
[20] C. N. Baroud, F. Okkels, L. Ménétrier, and P. Tabeling, Phys. Rev. E **67**, 060104 (2003).
[21] M. Chacron and I. L'Heureux, Phys. Lett. A **263**, 70 (1999).
[22] J. W. Cahn and J. E. Hilliard, J. Chem. Phys. **28**, 258 (1958); J. W. Cahn, Acta Metall. **9**, 795 (1961).
[23] P. C. Hohenberg and B. I. Halperin, Rev. Mod. Phys. **49**, 435 (1977).
[24] A. Volford, I. Lagzi, F. Molnár, and Z. Rácz, Phys. Rev. E **80**, 055102(R) (2009).
[25] J. D. Gunton, M. San Miguel, and P. S. Sahni, in *Phase Transitions and Critical Phenomena*, edited by C. Domb and J. L. Lebowitz (Academic, London, 1983), Vol. 8.
[26] See Supplemental Material at http://link.aps.org/supplemental/10.1103/PhysRevLett.110.078303 for (i) a detailed model description, (ii) movies on precipitate formation in 2D simulations, and (iii) examples of the results of 3D simulations.
[27] B. Chopard, P. Luthi, and M. Droz, Phys. Rev. Lett. **72**, 1384 (1994).
[28] P. Hantz and I. Biró, Phys. Rev. Lett. **96**, 088305 (2006).
[29] E. M. Foard and A. J. Wagner, Phys. Rev. E **85**, 011501 (2012).
[30] Z. Rácz, Physica (Amsterdam) **274A**, 50 (1999).
[31] Computations for a 3D tube are also possible but exceedingly time consuming. An example of a helicoid obtained in 3D is shown in Ref. [26].